공학석사 학위논문

Enhanced Battery Performance of Disordered Carbon and Graphene Double Coated SnO_2 Hollow Spheres

비정질 카본과 그라핀 이중 코팅을 통한

주석 산화물 중공구의 향상된 배터리 특성

2015 년 2 월

서울대학교 대학원

재료공학부

우 형 섭

Enhanced Battery Performance of Disordered Carbon and Graphene Double Coated SnO_2 Hollow Spheres

비정질 카본과 그라핀 이중 코팅을 통한

주석 산화물 중공구의 향상된 배터리 특성

지도교수 박 병 우

이 논문을 공학석사 학위논문으로 제출함.
2015 년 2 월

서울대학교 대학원
재료공학부
우 형 섭

우형섭의 공학석사 학위논문을 인준함.

2015 년 2 월

위 원 장 김 미 영
부위원장 박 병 우
위 원 강 기 석
위 원 문 태 호

Abstract

Innovative development of IT technology has resulted in an explosive usage of portable electronic devices and in modern life. Besides, obtaining green energy and storing it have emerged as an important issue due to environmental problems. To fulfill the crucial requirements of energy sources of these days, high-performance batteries, which are essential for the wide range of electro-technology, from the electronic devices to vehicles, have been researched.

Li-ion batteries are currently the most used energy storage device. Many anode materials for Li-ion battery are actively studied to overcome the low capacity limit of carbon material. SnO_2 is one of the most attractive candidate for anode materials with high capacity, but it has volume expansion problem inducing pulverization of electrode material during cycling. In this research, disordered carbon and reduced graphene oxide are doubly coated to SnO_2 hollow spheres which consist of SnO_2 nanoparticles. Conformal carbon and reduced graphene oxide coating provide SnO_2 hollow spheres with electronic pathway and buffer effect to prevent electrical losses of electrode.

SnO_2 hollow spheres are simply synthesized by hydrothermal method and also carbon coting is also modified by hydrothermal method. And then APTES surface modification is applied on carbon coated SnO_2 hollow spheres to coat tightly with graphene oxide through electrostatic interaction. Coated disordered carbon layer provide an electronic pathway to inner space of hollow sphere through porous hollow shell. Reduced graphene layer wrap several SnO_2 hollow spheres which provides electronic path to the entire electrode. Effect of each coating material enhances the battery performance of SnO_2 hollow spheres.

Keywords: Li-Ion Batteries, SnO_2 Hollow Spheres, Disordered Carbon, Reduced-Graphene Oxide, Anode.

Student Number: 2013-20610

Table of Contents

List of Figures

Chapter 1.

Chapter 2.

List of Tables

Chapter 1. Overview of Li-Ion Batteries

1.1. Introduction to Li-Ion Batteries

The lithium ion battery is a device that converts chemical energy into electrical energy and it refers to secondary battery due to reusable property via the repeated insertion and extraction of lithium ions to the electrode [1-3]. Because only Li^+ moves between electrodes in the cell, it is called "rocking chair battery" [4]. The lithium ion battery is composed of anode, cathode, electrolyte, and separator, which divides each electrode both physically and electrically. The maximum amount of generated work of lithium ion battery is equal to that of work obtained at equilibrium, and is the same as the Gibbs free energy change of the cell for an electrochemical reaction. The voltage of the circuit determined from the lithium chemical potentials of each cell is shown in Fig. 1-2.

$$V_{OC} = -\frac{\mu_{Li}^{cathode} - \mu_{Li}^{anode}}{ze}$$

Therefore, V_{OC} of a cell will more appropriately be related to the difference of the lithium chemical potential between the cathode ($\mu_{Li}^{cathode}$) and anode (μ_{Li}^{anode}), where z and e are, respectively, the number of electrons transferred and electronic charge [5].

Cell voltage decrease gradually as lithium ions move from the anode to the cathode spontaneously during discharging. While charging or discharging, the electrolyte plays a role as an ion conductor carrying lithium ions between each electrode. Also, the migration of electron toward an external circuit which is the source of the electrical energy, should be enabled by blocking electron moving into electrolyte. Applying a higher voltage than that of driving force of spontaneous

reaction leads to a charging, in which ions and electrons moving in opposite directions. On this account, the chemical energy can be compensated by charging process, and the state of the cell is returned to be dischargeable [6-7].

Li-ion battery has been used widely as an energy source of portable electronic devices, since Sony has successfully commercialized of the cells using graphite as an anode and $LiCoO_2$ as a cathode. Considering the application to electric vehicles and future energy demands, higher energy density, power quality, reliability, long cycle life, and low prices will have to be achieved. In particular, a lot of progresses have been attained to modify the properties of the electrode materials which are directly related to the performance of the battery. Further development of simple and cheap synthesis methods and the application of a variety of nano-materials are highly required [8-11].

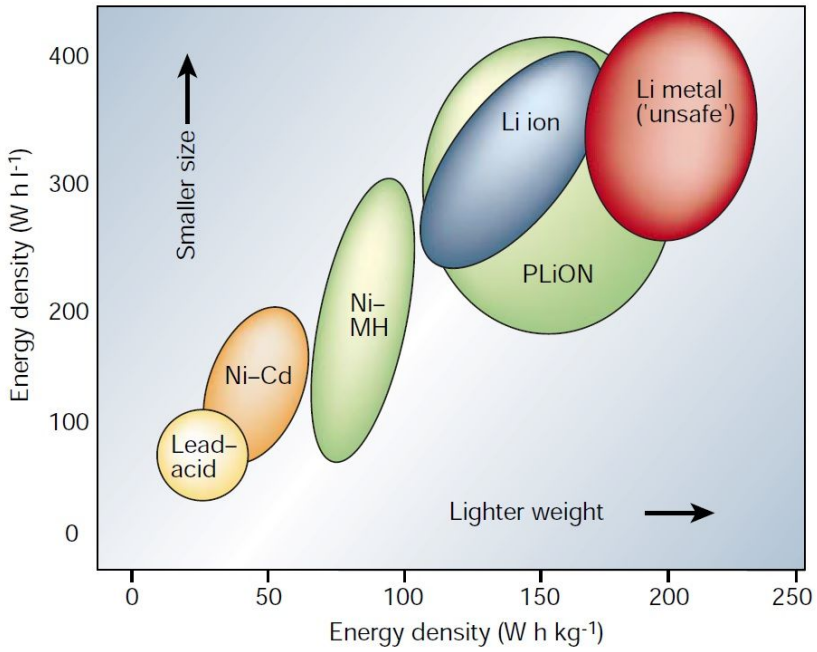

Fig. 1-1. (Color) Comparison of the different battery technologies in terms of volumetric and gravimetric energy density. From Ref. [1].

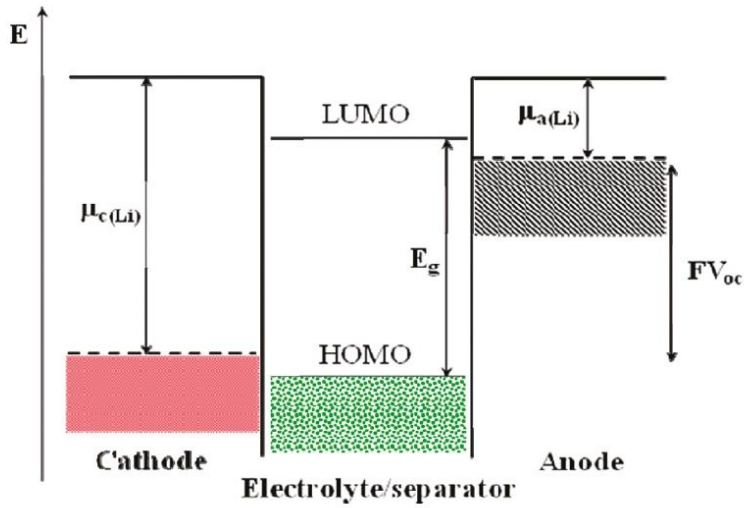

Fig. 1-2. (Color) Schematic energy diagram of a lithium cell at open circuit. $\mu_{a(Li)}$ and $\mu_{c(Li)}$ refer, respectively, to the lithium chemical potential in the anode and cathode. E_g refers to the band gap in the electrolyte. From Ref. [2].

1.2. Anode Material for Li-Ion Batteries: SnO_2

Lithium metal has been used as an anode material from the infancy of lithium secondary batteries. Even though lithium secondary batteries have advantage of high capacity, lithium metal has major safety problem that is internal short circuit formation caused by the dendritic growth of lithium during the repeated charging and discharging processes [12-13]. To overcome this problem, carbon-based materials were intensively studied as an anode material due to their unique properties [14]. For the case of graphite with the most basic type of carbonaceous material, lithium ions can be inserted continuously into its layered structure, with only about 10% of volume expansion, which enable a good cycle property. Furthermore, average reaction voltage of graphite is similar to that in lithium metal, therefore only slight loss of cell voltage is accompanying when lithium metal anode is replaced by graphite. However, the theoretical capacity of graphite anode is quite low (372 mAh/g) due to six carbons react with only one lithium in graphite. To enhance capacity of anode materials for lithium ion batteries, other materials (Si, Sn, Al, Ge, *etc.*) which form an alloy reaction with more lithiums have been widely investigated by many researchers [16-18].

Among them, tin metal has shown large volume capacity similar to that of lithium metal, and comparatively low operating voltage close to that of lithium metal anode. Since tin metal reacts with 4.4 lithiums, the theoretical capacity of tin metal reaches 994 mAh/g which is a lot higher than capacity of graphite [20]. However, because of the large volume expansion during cycling, cracks are formed by mechanical stress after prolonged cycling. These fractures lead to the decrease of reversible capacity, due to the dead materials detached from the electrodes and the generation of new SEI layers on newly exposed surfaces.

Since Idota *et. al.* [22] has reported amorphous tin-based composite oxide as anode, tin oxide have been received a lot of attention as an anode material due to their

large capacity, environmental benignity, and lower price. The reaction mechanism of the tin oxide goes through two steps as follows:

$$SnO_2 + 4Li^+ + 4e^- \rightarrow 2Li_2O + Sn$$

$$Sn + 4.4Li^+ + 4.4e^- \leftrightarrow Li_{4.4}Sn$$

After Dahn *et. al.* [23] was firstly suggested the reaction of tin oxide in 1997, the first reaction is a reduction process of tin oxide to tin metal, which has been known as an irreversible reaction. The second reaction is typical tin metal alloy reaction with lithium. In most cases, cells lose half of the capacity in the initial reaction due to its irreversible reaction with lithium, thus the major reaction of SnO_2 is the alloy reaction with lithium ($Li_{4.4}Sn$) in Fig. 1-3 [20-21]. But in recent studies, there are reports that the reaction of tin oxide with nano-size and high electronic conductivity environment could be fully reversible [28-29]. If all the processes are reversible, the tin oxide reacts with total 8.4 number of lithium ions which corresponds to 1491 mAh/g of theoretical capacity.

Huang's group observed the lithiation process of tin oxide nanowire by in situ TEM measurement in 2010 [24]. This revealed not only the total volume expansion 250 % during the lithiuation reaction with 90 % in longitudinal and 35 % in radial direction, but also Sn nano-sized particles are embedded in amorphous Li_2O matrix during the initial reduction of tin oxide into tin metal. This amorphous Li_2O matrix is known to relieve the volume expansion of the Sn metal (Fig. 1-4). Nonetheless, Tin oxide electrodes are not completely free from the capacity degradation due to volume change as Sn nanoparticle become larger aggregating themselves [24], so various studies, such as diverse nanostructures and carbon composites, have been proceeded in order to solve this problem by many groups [28-30, 32-37].

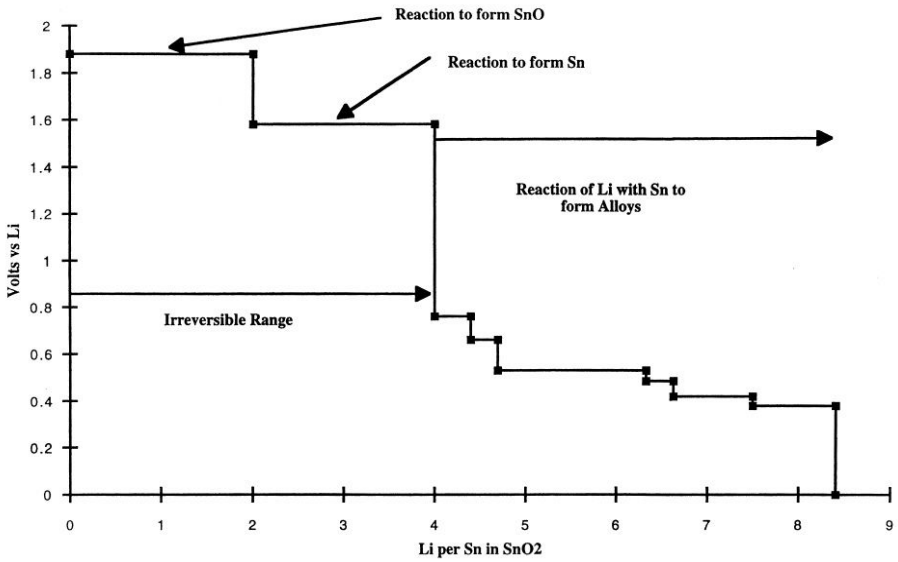

Fig. 1-3. Theoretical titration curve for reaction of lithium with SnO_2. From Ref. [21].

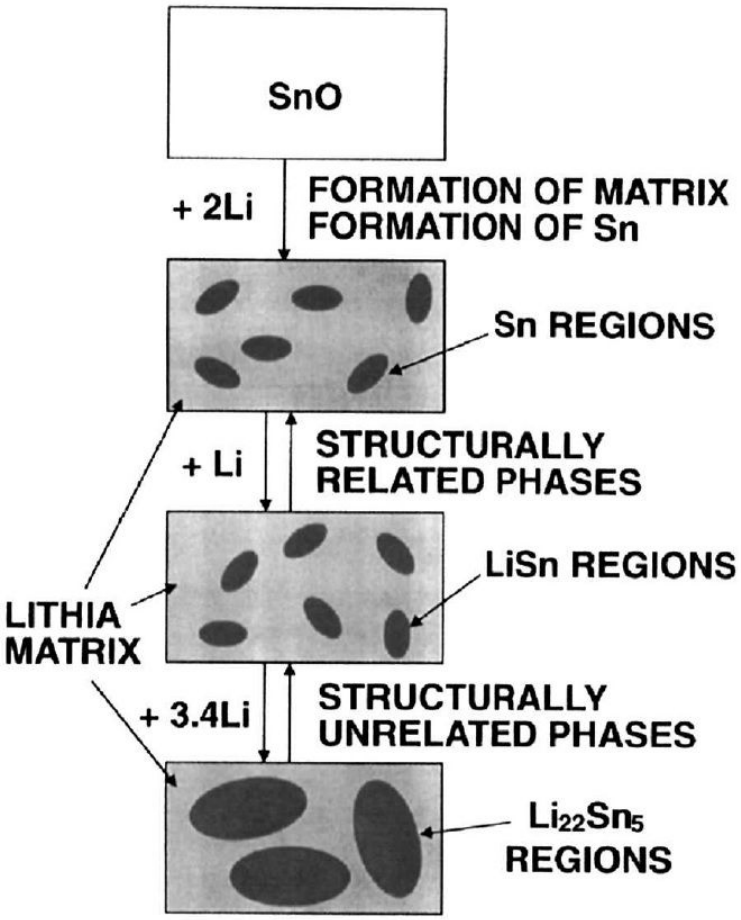

Fig. 1-4 Reaction mechanism schematic for the reaction of lithium with tin oxide. From Ref. [23].

1.3. SnO_2 Nanostructure and Hollow Spheres

SnO_2 has a limitation for application to anode due to drastic capacity loss arising from high volume expansion (~300 %) during charging and discharging. A variety of nano-morphology and carbon-based composite have been conducted by many groups to apply SnO_2 as an anode replacing the graphite [25-27]. Reducing the particle size to nano-scale brought a decrease in the absolute volume expansion. At the point when SnO_2 reaches a critical size, which is mechanical failure do not occur, electrode is free to damage from the volume expansion during the cycling. Kim *et al.* examined several sizes of SnO_2 nanoparticles (~3, ~4, and ~8 nm), and they found that ~3 nm of SnO_2 nanoparticles render a reversible volume expansion of Sn nanoparticles [25].

Morphological efforts to accommodate the volume expansion of SnO_2 are also conducted by many groups. Lou *et al.* [32] reported a one-pot synthesis of SnO_2 hollow nanospheres in Fig. 1-5. The synthesis was performed in a mixed solvent of ethanol and water using potassium stannate (K_2SnO_3) as the precursor and urea as an additive. The hollow structured SnO_2 was formed during the Inside-out Ostwald ripening process. SnO_2 hollow spheres demonstrated excellent electrochemical performance. At a rate of 0.2 C, when charged to 2 V, a specific capacity of 1140 mAh/g was observed after 30 cycles, which was higher than the theoretical value based on tin alloyed and de-alloyed with a lithium in Fig. 1-6. [32]. Hollow structure shows better cycle property compare to nanoparticle system, but still has a bad cyclability to use as an anode.

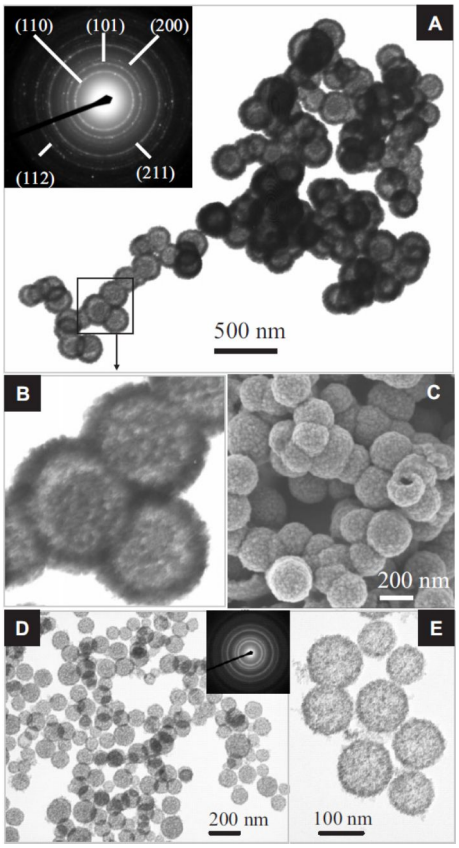

Fig. 1-5 TEM image (a) selected area electron diffraction (SAED) pattern (inset), and field-emission scanning electron microscopy (FESEM) image (c) of core/shell-type SnO_2 hollow nanostructures synthesized at 150 ℃ for 24 h. (b) A magnified TEM image corresponding to the highlighted in (a). (d,e) TEM images of SnO_2 hollow nanospheres synthesized under the same condition. From Ref. [32].

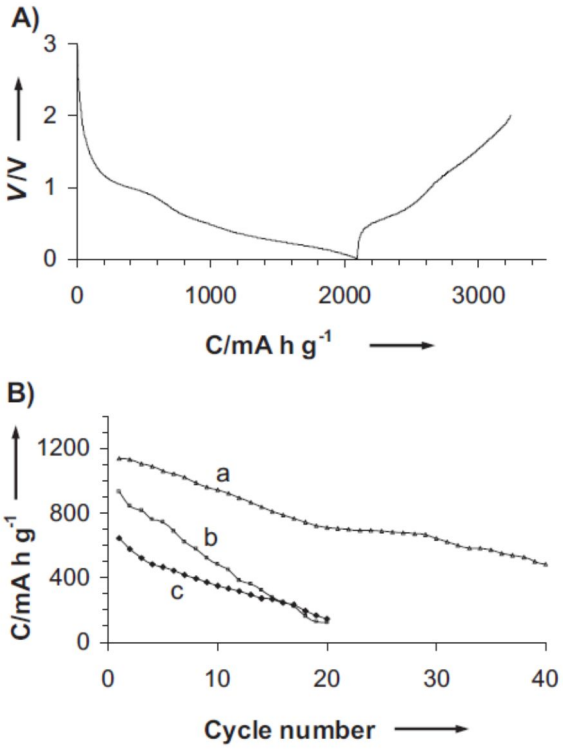

Fig. 1-6 A) First cycle charge–discharge curve of SnO_2 hollow nanospheres. B) Cycling performance of SnO_2 hollow nanospheres in the current work (a); SnO_2 hollow spheres (b); and pristine SnO_2 nanoparticles from reference [32].

1.4. Carbonaceous material modified SnO_2 anode

Furthermore, enhancing electrochemical properties, carbon-based materials are added as a matrix or coating layer and these methods have been widely conducted by many researchers [28-32]. Enhanced mechanical stress tolerances of the composites with carbon help the SnO_2 achieve larger capacity and a better cycle life. Various approaches have been explored to produce SnO_2/C composite. The simplest way to obtain carbon modified composite is using hydrothermal method with organic precursors, such as glucose [33]. In case of SnO_2 hollow spheres, Lou *et al.* [34] performed carbon coating on SnO_2 hollow spheres by the hydrothermal method in Fig. 1-7. The silica nanospheres were used as a template to make SnO_2 hollow spheres. At current density of 625 mA/g, a capacity of 625 mAh/g can be obtained after more than 100 cycles (voltage window is between 5 mV and 2 V).

Graphene has a very high surface area (theoretical value of 2620 m^2/g), electronic conductivity and good elasticity [38]. Graphene sheets distributed between the SnO_2 nanoparticles can prevent their direct contact and thereby minimize the aggregation and pulverization of the SnO_2 nanoparticles. Thus, Graphene wrapped SnO_2 nanoparticles perform an enhanced lithium storage properties compared to the pure SnO_2 nanoparticles are usually observed. Wang *et al.* [39] prepared SnO_2-graphene nan-composite by ternary self-assembly approaches (Fig. 1-8). The nanocomposite (60 wt. % SnO_2 and 40 wt. % graphene) showed a stable electrochemical cyclability. At a low current of 10 mA/g, a reversible capacity of 520 mAh/g was maintained over 100 cycles between 0.02 and 1.5 V.

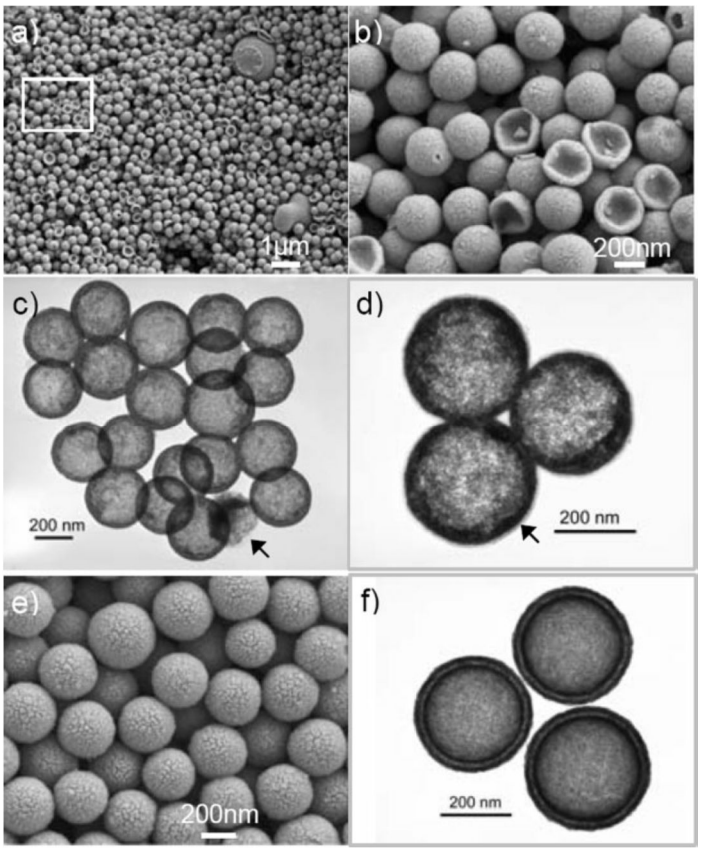

Fig. 1-7 (a,b) FESEM and (c,d) TEM images of SnO_2@carbon hollow spheres. Arrows in c) and d) indicate carbon shells, b) corresponds to the area indicated by a white rectangle in a). (e,f) Double-shelled SnO_2 hollow spheres. From Ref. [33].

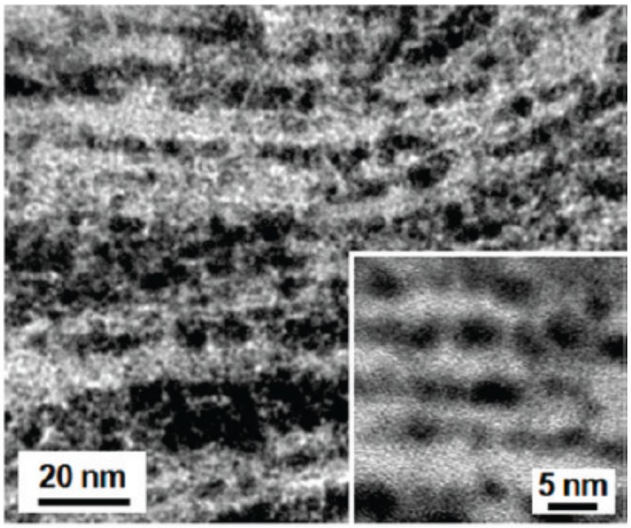

Fig. 1-8. Cross-sectional TEM images of a SnO_2-graphene nanocomposite film. Inset shows high-resolution TEM image in the nanocomposite film with alternating layers of nanocrystalline SnO_2 and graphene materials. From Ref. [39].

1.5. References

1. J.-M. Tarascon, "Issues and Challenges Facing Rechargeable Lithium Batteries," *Nature* **414**, 359 (2001).
2. P. Poizot, S. Laruelle, S. Grugeon, L. Dupont, and J.-M. Tarascon, "Nano-Sized Transition-Metal Oxides as Negative-Electrode Materials for Lithium-Ion Batteries," *Nature* **407**, 496 (2000).
3. F. T. Wagner, B. Lakshmanan, and M. F. Mathias, "Electrochemistry and the Future for the Automobile," *J. Phys. Chem. Lett.* **1**, 2204 (2010).
4. J. B. Goodenough and K.-S. Park, "The Li-Ion Rechargeable Battery: A Perspective," *J. Am. Chem. Soc.* **135**, 1167 (2013).
5. J. B. Goodenough and Y. Kim, "Challenges for Rechargeable Li Batteries," *Chem. Mater.* **22**, 587 (2010).
6. M. Winter, J. O. Besenhard, M. E. Spahr, and P. Novak, "Insertion Electrode Materials for Rechargeable Lithium Batteries," *Adv. Mater.* **10**, 725 (1998).
7. A. Manthiram and J. Kim, "Low Temperature Synthesis of Insertion Oxides for Lithium Batteries," *Chem. Mater.* **10**, 2895 (1998).
8. W. W. Lee and J.-M. Lee, "Novel Synthesis of High Performance Anode Materials for Lithium-Ion Batteries (LIBs)," *J. Mater. Chem. A* **2**, 1589 (2014).
9. A. S. Arico, P. Bruce, B. Scrosati, J.-M. Tarascon, and W. V. Schalkwijk, "Nanostructured Materials for Advanced Energy Conversion and Storage Devices," *Nat. Mater.* **4**, 366 (2005).
10. C. Jiang, E. Hosono, and H. Zhou, "Nanomaterials for Lithium Ion Batteries," *Nanotoday* **1**, 28 (2006).
11. Y. Wang, H. Li, P. He, E. Hosono, and H. Zhou, "Nano Active Materials for Lithium-Ion Batteries," *Nanoscale* **2**, 1294 (2010).
12. A. Manthiram, "Material Challenges and Opportunities of Lithium Ion Batteries," *J. Phys. Chem. Lett.* **2**, 176 (2011).

13. F. Cheng, J. Liang, Z. Tao, J. Chen, "Functional Materials for Rechargeable Batteries," *Adv. Mater.* **23**, 1695(2011).
14. J.-I. Yamaki and S.-I. Tobishima, in Handbook of Battery Material, ed. C. Daniel and J. O. Bessenhard, Wiley-VCH Verlag & Co. KGaA, Weinheim, Germany, 2011, ch. 13.
15. C. Wang, D. L. Wang and C. S. Dai, "High-Rate Capability and Enhanced Cyclability of Rechargeable Lithium Batteries Using Foam Lithium Anode," *J. Electrochem. Soc.* **A390**, 155 (2008).
16. F. Orsini, A. D. Pasquier, B. Beadudoin, J. M. Tarascon, M. Trentin, N. Langenhuizen, E. De Beer, P. Notten, "In Situ Electron Microscopy (SEM) Observation of Interfaces within Plastic Lithium Batteries," *J. Power Sources* **76**, 19 (1998).
17. A. N. Dey, "Electrochmeical Alloying of Lithium in Organic Electrolytes," *J. Electrochem. Soc.* **118**, 1547 (1971).
18. R. A. Huggins, "Lithium Alloy Negative Electrodes Formed from Convertible Oxides," *Solid State Ionics* **113,** 57 (1998).
19. C.-M. Park, J.-H. Kim, H. Kim, and H.-J. Sohn, "Li-Alloy Based Anode Materials for Li Secondary Batteries," *Chem. Soc. Rev.* **39**, 3115 (2010).
20. J. Sangster and C. W. Bale, "The Li-Sn (Lithium-Tin) System" *Journal of Phase Equilibria* **19**, 70 (1998).
21. J. Chouvin, J. Olivier-Fourcade, J. C. Jumas, B. Simon, and O. Godiveau, "Sn Mossbauer Study of Li_xSn Alloys Prepared Electrochemically," *Chem. Phys. Lett.* **308**, 413 (1999).
22. Y. Idota, T. Kubota, A. Matsufuji, Y. Maekawa, and T. Miyasaka, "Tin-Based Amorphous Oxide: A High-Capacity Lithium-Ion-Storage Material," *Science* **276**, 1395 (1997).

23. I. A. Coutney and J. R. Dahn, "Electrochemical and In Situ X-Ray Diffraction Studies of the Reaction of Lithium with Tin Oxide Composites," *J. Electrochem. Soc.* **144**, 2045 (1997).
24. J. Y. Huang, L. Zhang, C. M. Wan, J. P. Sullivan, W. Xu, L. Q. Zhang, S. X. Mao, N. S. Hudak, X. H. Liu, A. Subramanian, H. Fan, L. Qi, A. Kushima, and J. Li, "In Situ Observation of the Electrochemical Lithiation of a Single SnO_2 Nanowire Electrode," *Science* **330**, 1515 (2010).
25. C. Kim, M. Noh, M. Choi, J. Cho, and B. Park, "Critical Size of a Nano SnO_2 Electrode for Li-Secondary Battery," *Chem. Mater.* **17**, 3297 (2005).
26. C. T. Cherian, M. V. Reddy, S. C. Haur, and B. V. R. Chowdari, "Facile Synthesis and Li-Storage Performance of SnO Nanoparticles and Microcrystals," *RSC Adv.* **3**, 3118 (2013).
27. R. Demir-Cakan, Y.-S. Hu, M. Antonietti, J. Maier, and M.-M. Titirici, "Facile One-Pot Synthesis of Mesoporous SnO_2 Microspheres via Nanoparticles Assembly and Lithium Storage Properties," *Chem. Mater.* **20***,* 1227 (2008).
28. X. Zhou, L.-J. Wan, and Y.-G. Guo, "Binding SnO_2 Nanocrystals in Nitrogen-Doped Graphene Sheets as Anode Materials for Lithium-Ion Batteries," *Adv. Mater*. **25**, 2152 (2013).
29. X. W. Luo, X. P. Fang, Y. Sun, L. Y. Shen, Z. X. Wang, and L. Q. Chen, "Lithium Storage in Carbon-Coated SnO_2 by Conversion Reaction," *J. Power Sources* **226**, 75 (2013).
30. X. W. Lou, D. Deng, J. Y. Lee, and L. A. Archer, "Preparation of SnO_2/Carbon Composite Hollow Spheres and Their Lithium Storage Properties," *Chem. Mater.* **20**, 6562 (2008).
31. A. Manthiram, "Materials Challenges and Opportunities of Lithium Ion Batteries," *J. Phys. Chem. Lett.* **2,** 176 (2011).

32. X. W Lou, Y. Wang, C. Yuan, J. Y. Lee, and L. A. Archer, "Template-Free Synthesis of SnO_2 Hollow Nanostructures with High Lithium Storage Capacity," *Adv. Mater*. **18**, 2325 (2006).
33. X. Sun, J. Liu, and Y. Li, "Oxides@C Core-Shell Nanostructures: One-Pot Synthesis, Rational Conversion, and Li Storage Property," *Chem. Mater*. **18**, 3486 (2006).
34. X. W. Lou, C. M. Li, and L. A. Archer, "Designed Synthesis of Coaxial SnO2@carobn Hollow Nanospheres for Highly Reversible Lithium Storage," *Adv. Mater.* **21**, 2536 (2009).
35. X. W. Lou, "SnO_2 Nanoparticles with Controlled Carbon Nanocoating as High-Capacity Anode Materials for Lithium-Ion Batteries," *J. Phys. Chem. C* **113**, 20504 (2009).
36. S. Ding, Z. Wang, S. Madhavi, and X. W. (David) Lou, "SBA-15 Derived Carbon-Supported SnO_2 Nanowire Arrays with Improved Lithium Storage Capabilities," *J. Mater. Chem.* **21**, 13860 (2011).
37. X. Yu, S. Yang, B. Zhang, D. Shao, X. Dong, Y. Fang, J. Li, and H. Wang, "Controlled Synthesis of SnO_2@Carbon Core-Shell Nanochains as High-Performance Anodes for Lithium-Ion Batteries," *J. Mater. Chem.* **21**, 12295 (2011).
38. L.-S. Zhang, L.-Y. Jiang, H.-J. Yan, W. D. Wang, W. Wang, W.-G. Song, Y.-G. Guo, and L.-J. Wan, "Mono Dispersed SnO_2 Nanoparticles on Both Sides of Single Layer Graphene Sheets as Anode Materials in Li-Ion Batteries," *J. Mater. Chem*. **20**, 5462 (2010).
39. D. Wang, R. Kou, D. Choi, Z. Yang, Z. Nie, J. Li, L. V. Saraf, D. Hu, J. Zhang, G. L. Graff, J. Liu, M .A. Pope, and I. A. Aksay, "Ternary Self-Assembly of Ordered Metal Oxide-Graphene Nanocomposites for Electrochemical Energy Storage," *ACS Nano* **4**, 1587 (2010).

Chapter 2.

Disordered Carbon and Reduced Graphene Oxide Coating on the SnO_2 Hollow Spheres

2.1. Introduction

As mentioned before, unique nanostructure and adoption of carbon coating have huge advantages to design SnO_2 electrode. Ideally, the optimum amount of the carbon content should be determined by considering the size and structure of SnO_2. Without its optimum amount of carbon content, many studies show high carbon contents (above 50 wt. %) in their composite [1-6]. It seems the high amount of carbon material in the electrode means the high electrical contact probability between broken SnO_2 and current collector, sustaining its structural uniformity of electrode. A rigid and uniform carbon coating makes anode electrode possible to remain initial morphology for a long cycle with a good electronic path. But very high carbon content decrease the cell performance because thick carbon layer which has lower quality of sp^2 domain hindering Li ion diffusivity [1]. Also, the high loading of carbon materials lead low theoretical capacity which combination of carbon (graphite, 372 mAh/g) and SnO_2 (782 mAh/g) [8]. Therefore, lower carbon content is require to obtain high theoretical capacity and also uniform carbon coating on unique nano-morphology for longer cycle life.

Mullen *et al.* [9] showed graphene encapsulation on the metal oxide has lowered carbon loading amount less than 10 wt. % and tight contact of graphene layer and metal oxide has much higher capacity properties. In this study, we apply both disordered carbon and reduced graphene oxide on the hollow spheres which consist of 10 nm-size tin oxide nanoparticles. Hydrothermal method is an easy way to modify

each primary particle with carbon layer. But, SnO_2 reduced Sn metal above 550 ℃ through carbothermic reduction [7-8], it results the formation of disordered carbon was formed, which is not enough to well organize sp^2 domains well. Due to the limit of carbonization temperature, graphene was adopted to provide entire cell with reasonable electrical conductivity even at low carbonization temperature. Both disordered carbon and graphene have seen the impact on improving tin oxide hollow sphere's cycle performance, with low carbon contents even less than 10 wt. %.

2.2 Experimental Section

Preparation of RGO/C/ SnO_2 hollow spheres: A simple hydrothermal method was adopted to synthesize SnO_2 hollow spheres using K_2SnO_3 as a precursor and ethanol/D·I water solution [9]. Mix anhydrous 18.75 ml of ethanol and 31.25 ml of D. I. water (37.5 vol. %), and $K_2SnO_3 \cdot 3H_2O$ (240 mg) and Urea (300 mg) was then added to solution. They were stirred under magnetic stirring for 30 min until the solution becomes translucent. Solution is then transferred to a 100 ml Teflon-lined stainless steel autoclave at 180 ℃, 24 h. After cooling to room temperature, the resulting precipitates were washed a couple of time in D. I. water, followed by drying in oven for 10 h.

Carbon coating was conducted through hydrothermal carbonization. SnO_2 hollow spheres (200 mg) and anhydrous glucose (133 mg, 40 wt. %) were added into D. I. water (25 ml). They were stirred for 1 h with 5 min sonication. And then, solution is transferred to a 100 ml Teflon-lined stainless steel autoclave at 180 ℃ for 4 h [7,10]. After cooling in room temperature, the resulting precipitates were washed a couple of times in D. I. water, followed by drying in oven for 10 h. As obtained carbon coated sample was heat-treated under Ar atmosphere at 500℃ for 3 h.

GO was synthesized from natural graphite flakes (325 mesh, Aldrich) by a modified Hummers' method [11]. The obtained SnO_2 hollow spheres (200 mg) were dispersed into absolute ethanol (200 ml) via sonication. After 2 ml of aminopropyltrimethoxysilane (APTES) was poured into the above solution, and the solution was stirred for 12 h to obtain APTES-modified SnO_2 hollow spheres [12]. The fabrication of graphene oxide coated SnO_2 hollow spheres was rendered by an electrostatic interaction between positively charged APTES-modified SnO_2 and negatively charged GO. For an assembly, the APTES-modified SnO_2 dispersion (1 mg/mL) was added into an aqueous graphene oxide solution (0.1 mg/mL) under

magnetic stirring for 2 h with 5 min sonication. As obtained GO coated sample was heat-treated under Ar atmosphere at 500 ℃ for 3 h.

As obtained hydrothermally carbon coated SnO_2 hollow spheres (before 500 ℃ annealing) were modified by APTES as same concentration at GO coting to bare SnO_2 hollow spheres. Carbon coated SnO_2 hollow spheres (200 mg) were dispersed into absolute ethanol (200 ml) via sonication. After 2 ml of aminopropyltrimethoxysilane (APTES) was poured into the above solution, and the solution was stirred for 12 h to obtain APTES-modified carbon SnO_2 hollow spheres (before annealing at 500 ℃). The fabrication of reduced graphene oxide coated C/SnO_2 hollow spheres was also rendered by an electrostatic interaction between positively charged APTES-modified C/SnO_2 and negatively charged GO. As same as the RGO/SnO_2 HS, the APTES-modified C/SnO_2 dispersion (1 mg/mL) was added into an aqueous graphene oxide solution (0.1 mg/mL) under magnetic stirring for 2 h. As obtained GO and carbon coated sample was heat-treated under Ar atmosphere at 500 ℃ for 3 h.

Materials Characterization: The crystal structure and grain size of the SnO_2 hollow spheres were characterized by x-ray diffraction (XRD, D8 Advance: Bruker). The morphology was analyzed using a scanning electron microscopy (Merlin Compact), and carbon concentration was measured using a CHNS analyzer (Flash EA 1112: Thermo Electron Corp.). The nitrogen adsorption and desorption isotherm were obtained at 77K (Micromeritics ASAP 2010), and the specific surface area and the pore size distribution were calculated by the Brunauer-Emmet-Teller(BET) and the Barre-Joyner-Halenda(BJH) methods, respectively.

Electrochemical Measurement: For the electrochemical characterization, the active materials were tested by using coin type half cell (2016 type) with a Li counter electrode. The composition of the electrode was set to be the same for all of the samples, which consisted of an active material, super P carbon black, and a polyvinylidene fluoride (PVdF) binder with a weight ratio of 8:1:1, and the geometric area of the electrode was 0.71 cm^2. The electrolyte was prepared by mixing 1M

LiPF6 in ethylene carbonate and diethylene carbonate (1/1 vol. %) (Panax Etec). Electrochemical impedance spectra (EIS) and cyclic voltammetry were measured using a potentiostat (CHI 608C: CH Instrumental Inc.). The EIS was obtained after 5cycles at 1C and the frequency range is from 1 mHz to 100 kHz with an AC amplitude of 5 mV at 0.6 V. The cells were cycled between 5 mV and 1.2 V after the first discharge from the initial open-circuit voltage. The cycling tests were performed at 1 C (each value are different due to carbon contents). The specific capacity was calculated based on the amount of only SnO_2, and the capacity of carbon was subtracted in this article.

2.3. Result and Discussion

The synthetic processes for the RGO/C double-coated SnO_2 hollow sphere (RGO/C/SnO_2 HS) are illustrated in Fig. 2-1. The hydrothermal method produced ~10-nm-size nanoparticles which consist of the porous hollow spheres. After carbon coating on each SnO_2 hollow sphere by hydrothermal method, the carbon-coated SnO_2 hollow sphere (C/SnO_2 HS) was wrapped by graphene oxide (GO) sheets by electrostatic interaction between positively-charged C/SnO_2 HS and graphene oxide interface prepared through the surface modification by APTES and negatively-charged GO through pH control. Annealing process after GO wrapping gives rise to the reduced graphene oxide (RGO), resulting three-dimensional network that renders well-connected electron percolation among the C/SnO_2 HS.

The XRD patterns of carbon-material modified samples are shown in Fig. 2-2. All diffraction peaks are indexed to SnO_2 with the space group of P42/mnm (136) (JCPDS #41-1445), and no secondary phases are detected. Peaks in diffraction pattern are broadened and it is an indicative of SnO_2 nanocrystals. The average grain size were estimated using Scherrer equation [13-16] with the FWHM (full width at half maximum) (fitted using a double peak Lorentzian function, considering the effect of Cu $K_{\alpha1}$ and $K_{\alpha2}$) corresponding to the (110), (101), (211) main peaks, and are tabulated in Table 2-1. The grain sizes of the samples modified with carbon material are larger than those of uncoated hollow spheres after calcination. Also, The graphene oxide layer also could prohibit the grain growth of SnO_2 during annealing process.

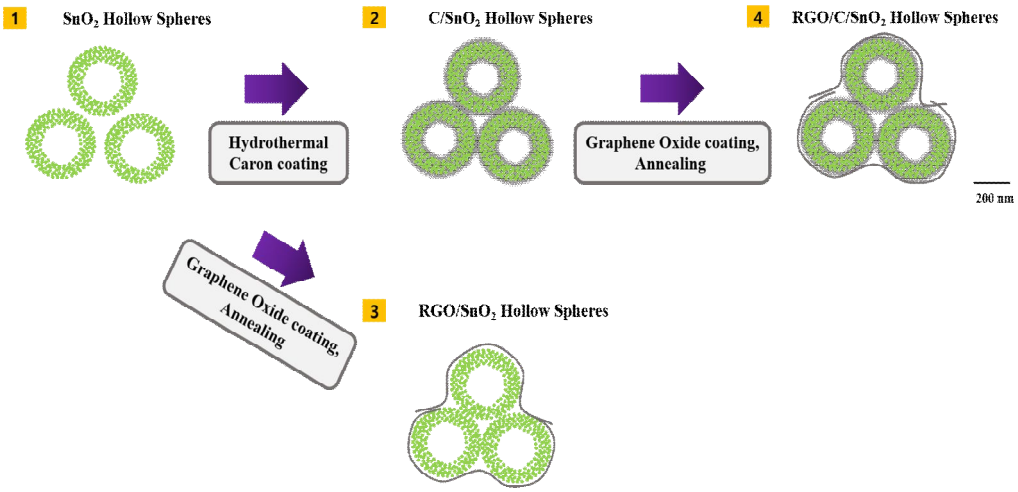

Fig. 2-1. (Color) The schematic image of synthetic processes for the RGO/C double-coated SnO_2 hollow spheres.

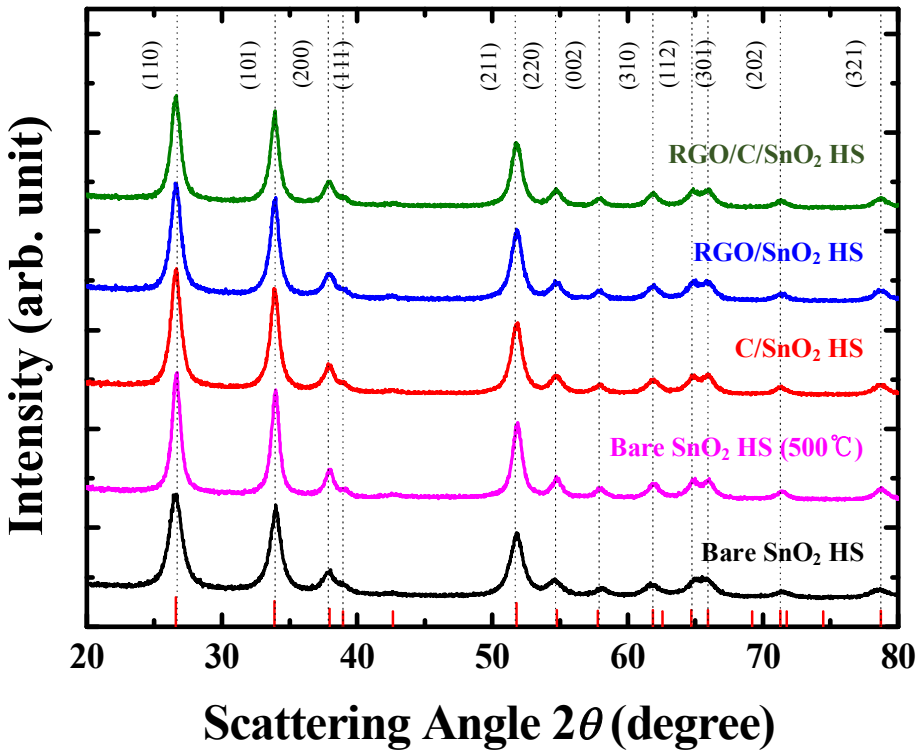

Fig. 2-2. (Color) XRD patterns of the SnO_2 hollow spheres with different carbon coating (red, blue and green color lines)and Bare SnO_2 hollow spheres (black color line), and Bare SnO_2 hollow spheres with annealing without carbon coating (pink color line).

To compare the carbon contents, CHNS analysis is performed and the results are shown in Table 2-1. Carbon contents between RGO modified sample and disordered carbon modified sample are similar to each other and the double coated sample are slightly higher than that of RGO or disordered carbon coated sample reasonably, but the amount is 7.7 wt. % of carbon. Calculated theoretical capacity considering only alloying reaction of Sn metal with Li of each samples are also in Table 2-1.

Several groups have been reported the carbon modified SnO_2 anode with high weight percent of carbon [20-24]. It is the obvious result that the carbon modification is the most well-known solution to alleviate the continuous capacity loss due to high volume expansion during charging and discharging. But the high carbon loading means the cell has a lower theoretical capacity as the carbon material has much lower theoretical capacity compare to oxide material. Therefore, it should be considered to find optimum carbon contents or minimum carbon amount. And some groups show the optimum carbon contents in their system [27-28]. Our results has very low carbon contents even though using both disordered carbon and reduced graphene oxide.

Sample	Grain size (nm)	C (wt. %)	Theoretical capacity (mAh/g)
RGO/C/SnO_2 HS (500 ℃)	15.5±1.8nm	7.7	750.4
RGO/SnO_2 HS (500 ℃)	14.6±1.9nm	4.86	762.0
C/SnO_2 HS (500 ℃)	14.3±1.6nm	5.36	760.0
SnO_2 HS (500 ℃)	19.8±1.3nm		
SnO_2 HS	9.2±0.77nm		782

Table 2-1. The carbon composition of carbon modified SnO_2 hollow spheres measured by CHNS elemental analysis, the grain size were estimated by x-ray diffraction, and the calculated theoretical capacity of each samples.

The scanning electron microscopy (SEM) images in Fig. 2-3 confirm that SnO_2 hollow spheres are well synthesized with 300～500 nm diameter with 80～90 nm shell thickness which consist of primary particle size is about 10 nm. The carbon coated SnO_2 hollow spheres are well structured sphere morphology which is similar to that of the bare sample. Graphene oxide is well coated both RGO/SnO_2 HS and RGO/C/SnO_2 HS. All carbon coated samples has primary particle size with about 15 nm after annealing at 500 ℃. Bare sample after annealing has primary particle size with about 20 nm, it means that the carbon coating layer act as a blocking layer to hinder the grain growth of SnO_2 nanoparticles during thermal reduction process.

The porous nanostructures of the SnO_2 hollow spheres are also confirmed by BET and BJH method (Fig. 2-4), showing a typical *type-IV* meso-porous structure [29-30]. The hollow spheres has porosity of average pore size of 3.62 nm and BET surface area of 66 m^2/g. The typical isotherm curve of SnO_2 hollow spheres are shown in Fig. From the BET analysis, pore size is large enough for the carbon source (glucose) in solution to penetrate into the inner space of SnO_2 hollow spheres and it is thought to fill the inner pore uniformly. Considering its primary particle size and carbon contents, the carbon coating layer is about 0.56 nm from simple calculation (hard carbon : ~1.5 g/cm^3, SnO_2: ~15 nm size), indicating carbon coating is enough to coating each nano-particles within the pores [31-32, 54]. Also, using BET surface area, the calculated carbon layer is about 0.572 nm similar to simple calculation. These porous nanostructure is beneficial for coating inside its space with electronic path way to inner space and these carbon coating could act as a buffer layer to minimize its aggregation during cycling.

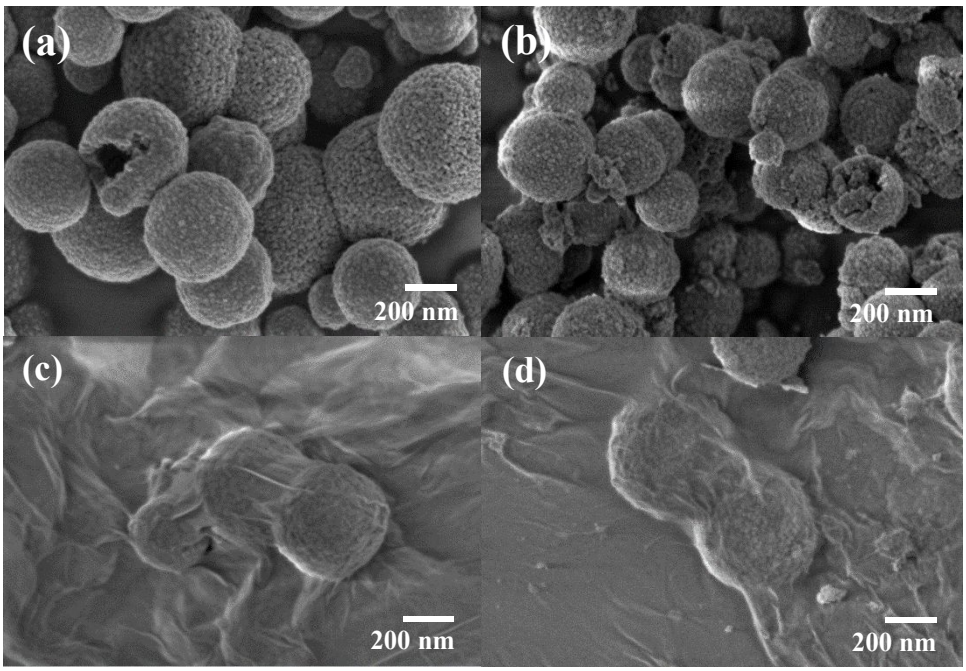

Fig. 2-3. SEM images of (a) Bare SnO_2 hollow spheres, (b) C/SnO_2 hollow spheres, (c) RGO/SnO_2 hollow spheres, (d) RGO/C/SnO_2 hollow spheres.

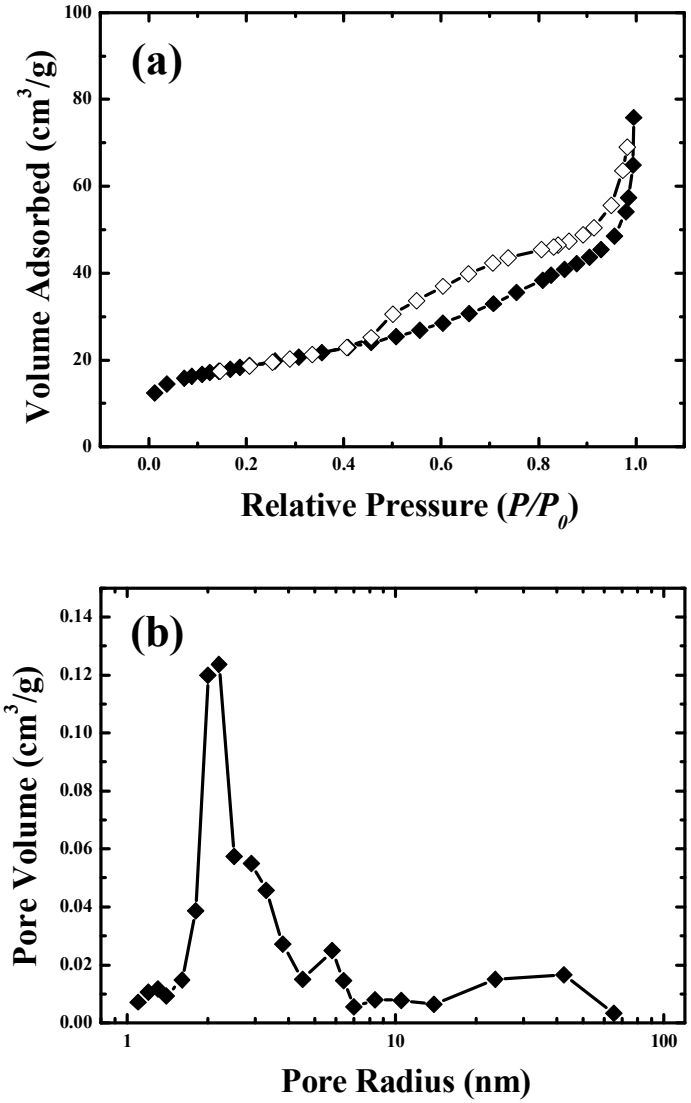

Fig. 2-4. (a) N_2 adsorption/desorption isotherm curve for the Bare SnO_2 hollow spheres. (b) The desorption pore size distribution of the Bare SnO_2 hollow spheres using the BJH method.

The Raman spectra of each samples are presented in Fig. 2-5. The Raman spectra of RGO/C/SnO_2 hollow spheres reveals both features of *D* band (~1370 cm^{-1}) and *G* band (~1600 cm^{-1}), and the spectrum of RGO/C/SnO_2 hollow spheres lies between the two samples, proving that the desired product is successfully modified by both the reduced graphene oxide and hydrothermally-derived disordered carbon [33, 46]. The calculated $I_{(D)}/I_{(G)}$ ratio of RGO/C/SnO_2 HS, RGO/SnO_2 HS, C/SnO_2 HS are respectively 0.86, 0.70, 0.68, and RGO/C/SnO_2 HS has an interval ratio value of RGO/SnO_2 HS and C/SnO_2 HS as consider its carbon contents ratio.

It is controversial issue that the reduced graphene oxide has higher $I_{(D)}/I_{(G)}$ ratio than that of graphene oxide. The origin of $I_{(D)}$ of RGO comes from the defect site and remained functional groups on the RGO surface when GO was reduced by thermal energy. Several groups have showed various result of $I_{(D)}/I_{(G)}$ ratio of reduced graphene oxide[33-45]. Some results shown the $I_{(D)}/I_{(G)}$ ratio rise after reducing process [33-39], but others shown opposite result [40-43]. Besides, There are the similar $I_{(D)}/I_{(G)}$ ratio before and after reduction of graphene oxide [44-45]. In case of disordered carbon, the small grain size of disordered carbon influence its $I_{(D)}$ its edge length is higher than plane area of it [46]. It's limitation of carbonization temperature (~550 ℃) due to the carbothermal reduction of SnO_2 to Sn metal is about 550 ℃.

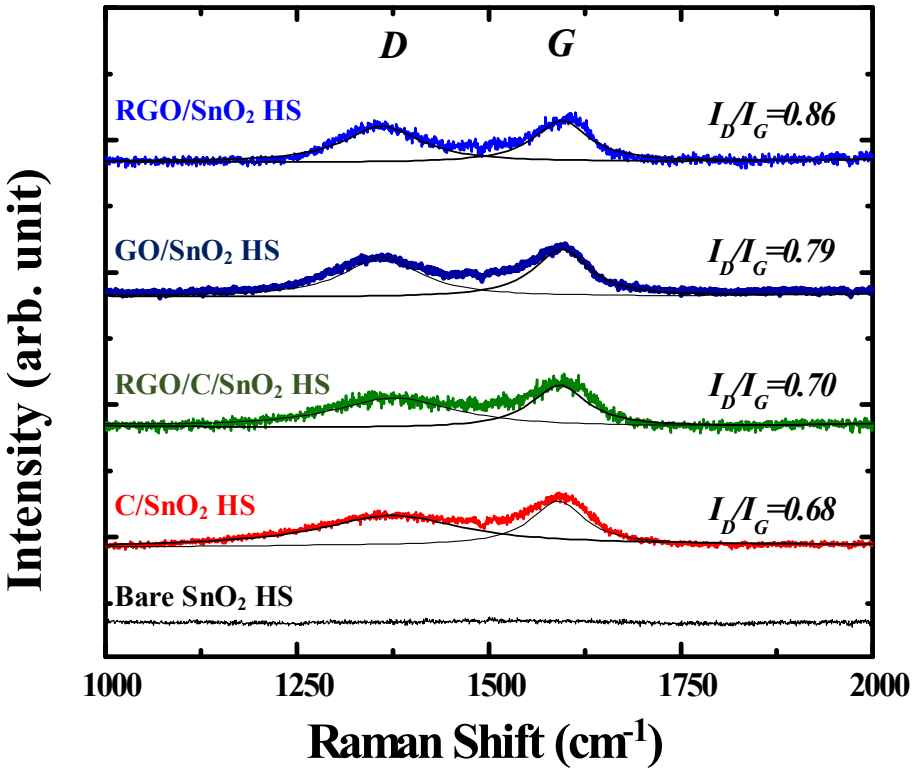

Fig. 2-5. (Color) Raman spectra of Bare SnO_2 hollow spheres, C/SnO_2 hollow spheres, GO/SnO_2 hollow spheres, RGO/SnO_2 hollow spheres, RGO/C/SnO_2 hollow spheres with fitted *D* and *G* bands.

The voltage profiles of RGO/C/SnO_2 HS, RGO/SnO_2 HS, C/SnO_2 HS, Bare SnO_2 HS are presented in Fig. All samples has a plateau under 1 V indicating the formation of first formation of Li_2O phase and Sn metal. After that, both alloy reaction of Sn metal with Li and intercaltion of Li ion into carbon layer has begun. The initial capacity loss after first cycle is came from SEI (Solid Electrolyte Interface) layer and formation of lithia. After first cycle, the reaction of cell is only alloy reaction of Sn metal embedded in the amorphous lithia with the voltage range is finished before reduction reaction of Sn metal to SnO_2.

Cyclic-voltammetry was conducted at voltage range 0.005 - 3 V. The full reaction of carbon modified SnO_2 HS sample is in Fig. 2-6. Compare to Bare SnO_2 HS and other carbon modified SnO_2 HS, all samples have the peak which indicate the reduction reaction of Sn metal over 1.2 V. Slightly difference between the peak is carbon modified sample are also second peak at near 2 V. So, the high conductivity environment help the reduction reaction of Sn metal to SnO_2 with nanosized. Such result of carbon composite was reported by several groups [8-13].

In this research, we are observed cell property at voltage under 1.2 V which means only use alloy reaction of Sn metal. So, the theoretical capacity of the SnO_2 set 782 mAh/g which is the reversible Sn metal reaction with Li. Each theoretical capacity was calculated by weight percent of carbon (SnO_2 (reversible capacity) × SnO_2 wt. % + Graphite × Carbon wt. %) in Table 2-1.

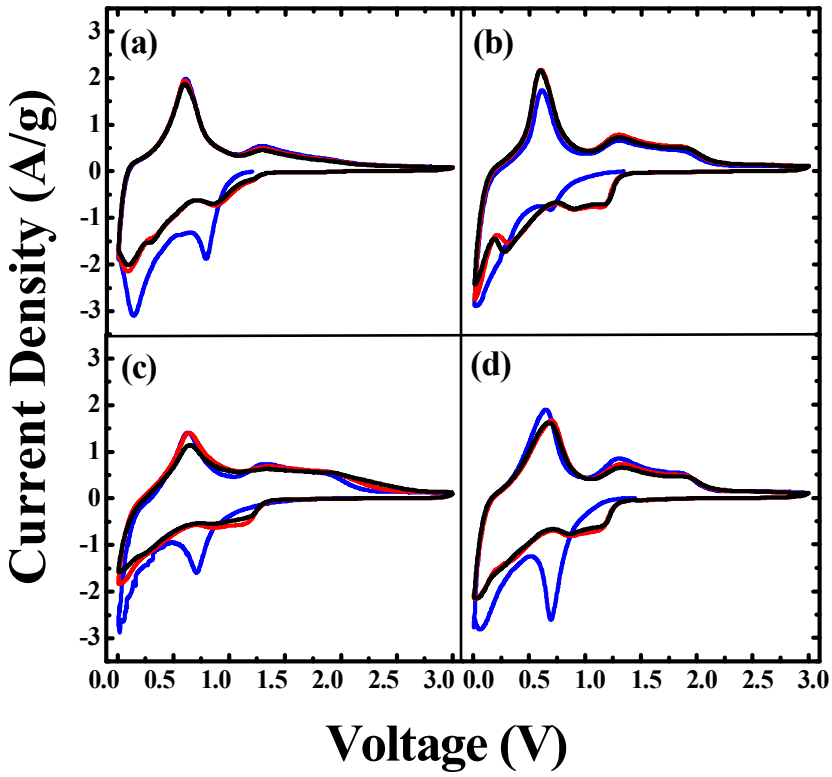

Fig. 2-6. (Color) The charge- and discharge-capacity retention of (a) Bare SnO_2 hollow spheres, (b) C/SnO_2 hollow spheres, (c) RGO/SnO_2 hollow spheres, (d) RGO/C/SnO_2 hollow spheres (0.005 - 3.0 V, scan rate is 0.5 mV/s).

To confirm the effects of each carbon coated samples, the electrochemical performance of the bare SnO_2 HS, C/SnO_2 HS, RGO/SnO_2 HS, and RGO/C/SnO_2 HS were galvanostatically cycled in the range of 0.005 - 1.2 V (vs. Li^+/Li) at a 1 C (Fig. 2-6). It seems that the bare SnO_2 hollow spheres suffer from a gradual capacity loss due to the aggregation of nanoparticles and detached from carbon matrix induced by volume expansion, and has only 50 mAh/g (after 100^{th} cycles). Comparing the carbon-modified composites, the capacity fading was more significant for the RGO/SnO_2 HS compared to the carbon modified SnO_2 HS, yielding a discharge capacity of 100 mAh/g at the 100^{th} cycle. Because of the absent of inner space coating, the inner part of the hollow spheres are vulnerable to pulverization and contact with electronic path. C/SnO_2 HS has a stable cycle properties after 100 cycles, but its capacity was lower than RGO modified C/SnO_2 HS due to low conductivity of disordered carbon. The RGO/C/SnO_2 HS, on the other hand, show more stable cycle-life performances, which indicates the disordered carbon layers effectively inhibit the massive aggregations of each SnO_2 nanoparticles during cycling. Also, the higher reversible capacity of the RGO/C/SnO_2 HS sample (ca. ~331.8 mAh/g after100 cycles) than that of the C/SnO_2 HS comes from the network of tightly-wrapped-graphene on C/SnO_2 HS, enhancing the electronic percolation within the hollow spheres.

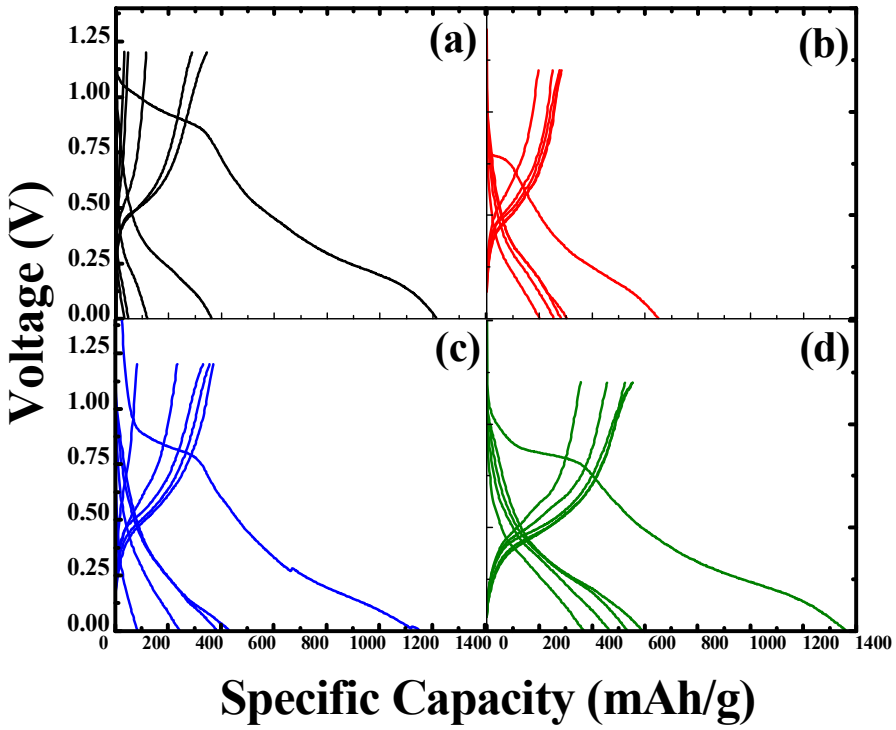

Fig. 2-7. (Color) The charge- and discharge- capacity retention of (a) Bare SnO_2 hollow spheres, (b) C/SnO_2 hollow spheres, (c) RGO/SnO_2 hollow spheres, (d) RGO/C/SnO_2 hollow spheres (0.005 - 1.2 V).

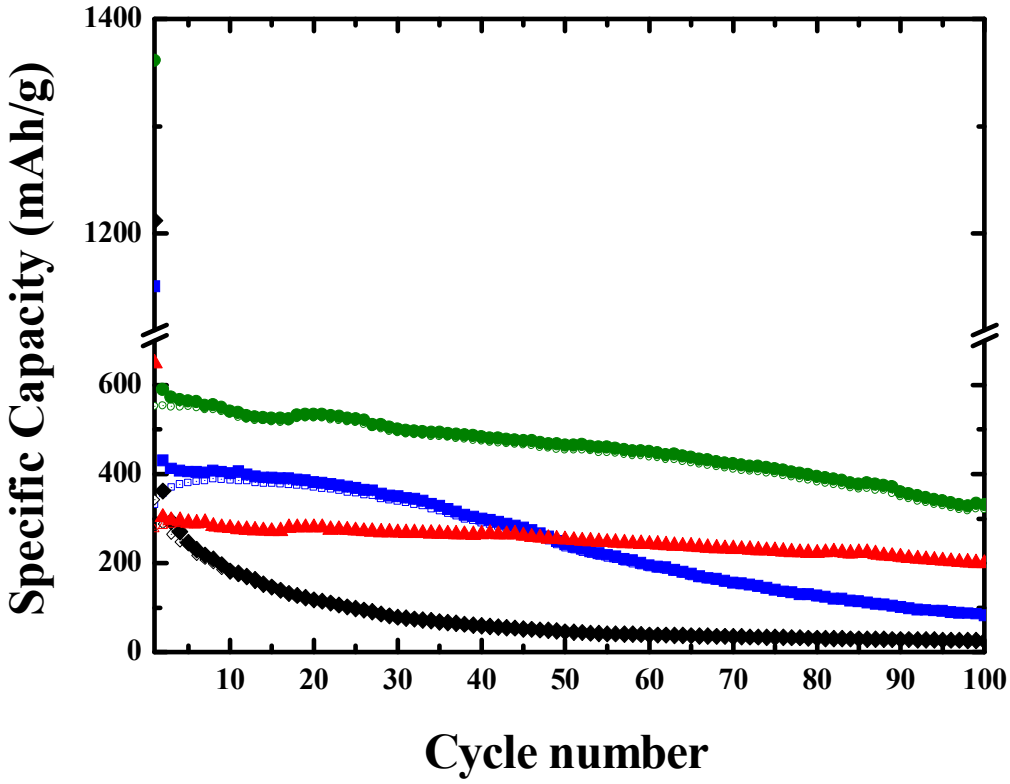

Fig. 2-8. (Color) Cycle-life performance of (a) Bare SnO_2 hollow spheres, (b) C/SnO_2 hollow spheres, (c) RGO/SnO_2 hollow spheres, (d) RGO/C/SnO_2 hollow spheres at 1C (0.005 - 1.2 V).

The rate capability of samples are in Fig 2-9. Reduced graphene oxide modified samples are much higher rate properties than disordered carbon modified sample. It is related to conductivity of sample, higher conductivity is able to much high rate properties with similar lithium ion movement though pores of samples.

Cell properties are related to an electrochemical reaction depends on charge transfer. Electrochemical impedance spectra of each samples are measured at the open potential of 0.6 V at the fifth discharge cycle. Compare the Nyquist plot in Fig. 2-10, all samples show one semicircle in the high frequency region and a straight slope (~ 45°) in the low frequency region. The diameter of semicircle reveals the impedances associated with the charge-transfer resistance (R_{ct}), which is important factors in electrochemical reaction [50-51]. Charge transfer resistance (R_{ct}) of both RGO/C/SnO_2 HS and RGO/SnO_2 HS is much smaller than that of C/SnO_2 HS and Bare SnO_2 HS, thus suggesting that RGO coating possesses lower contact and charge transfer resistance. It means the highly conductive 2-D graphene layer can facilitate electron transfer from each SnO_2 hollow spheres within the overall electrode [52, 54]. Double coated samples also has meso-pores which makes Li ion in the electrolyte can rapid diffusion, thus enhancing of electron conduction and ion transfer [53].

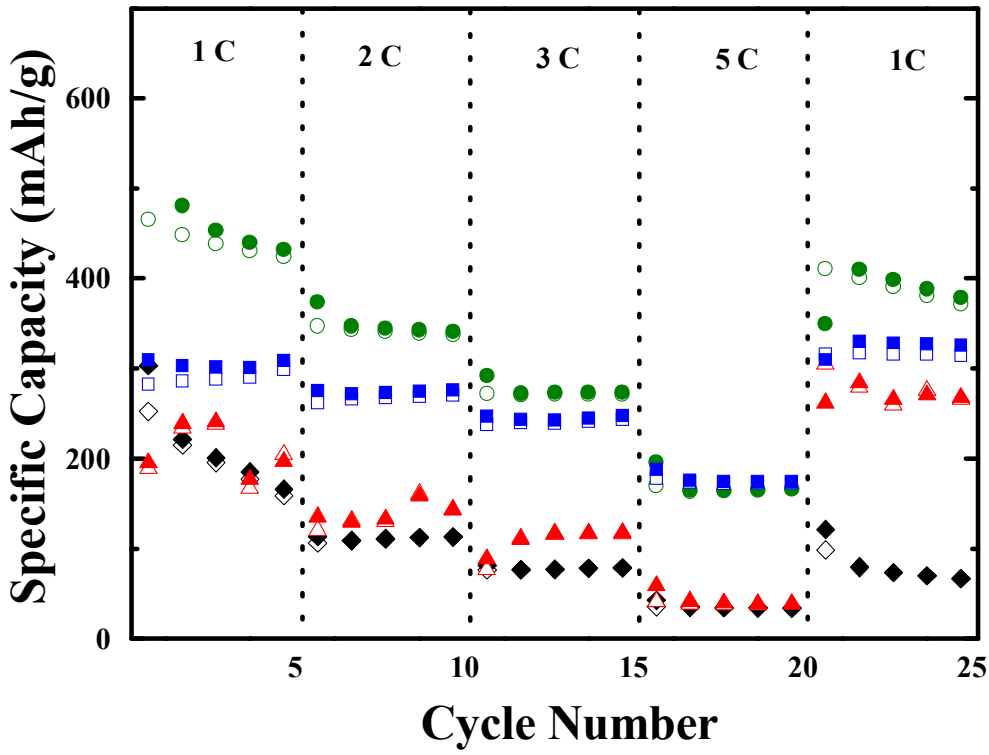

Fig. 2-9. (Color) Rate capability of (a) Bare SnO_2 hollow spheres, (b) C/SnO_2 hollow spheres, (c) RGO/SnO_2 hollow spheres, (d) RGO/C/SnO_2 hollow spheres at 1-5 C (0.005-1.2 V).

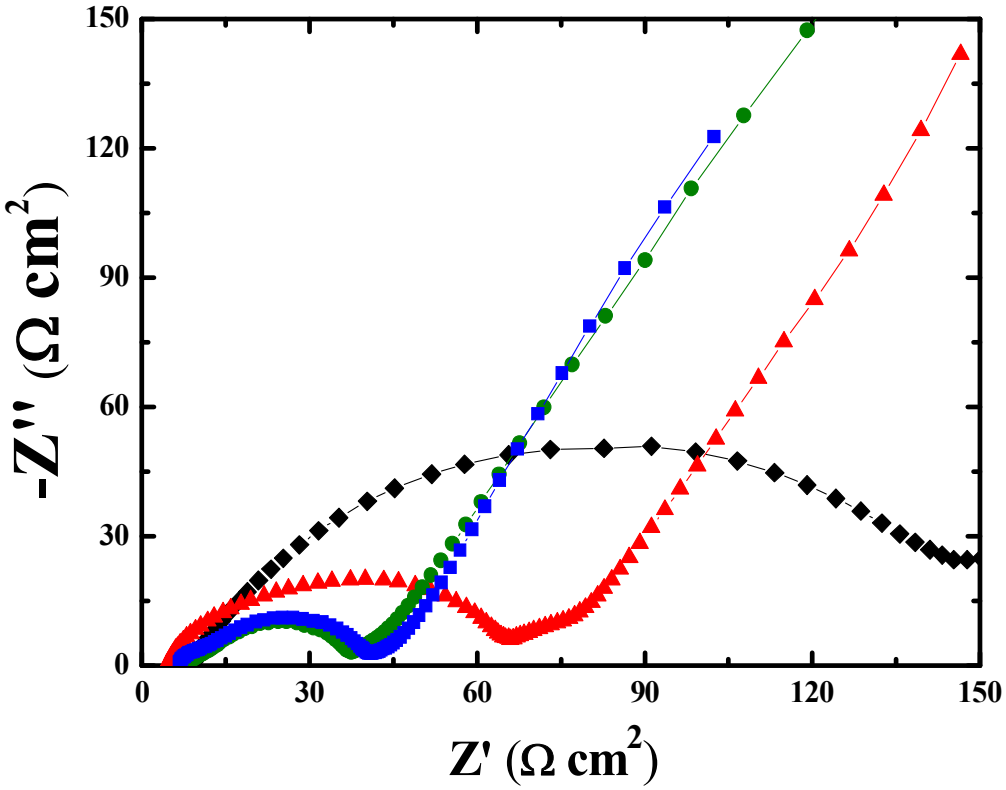

Fig. 2-10. (Color) Impedance Spectroscopy of (a) Bare SnO_2 hollow spheres, (b) C/SnO_2 hollow spheres, (c) RGO/SnO_2 hollow spheres, (d) RGO/C/SnO_2 hollow spheres at 0.6 V after 5 cycles.

2.4 Conclusions

In this work, we have proposed the RGO/C/SnO_2 hollow spheres as an anode material with excellent electrochemical properties. The hollow spheres are facilely modified through distinct carbon-based coating steps via conformal carbon coating, GO wrapping, and thermal reduction. The ~15-nm-sized RGO/C/SnO_2 hollow nano-composites with ~400-nm exhibited superior electrochemical performance including remarkable cycle life, high reversible capacity, and excellent rate capability even at 1 C. The enhanced electrochemical performance arose from the combination of unique properties of the meso-pores act as a coating site to relieve the volume expansion during cycling, conformal carbon layer on each nanoparticle surface buffers volume changes, and conductive RGO sheets connect the hollow spheres to each other. This work introduced the double coating strategy and it can extend the synthesis of other previous novel coating methods.

This research show very high capacity even at 1 C and the cut-off voltage up to 1.2 V as low as comparing other research of SnO_2. The carbon content are also very low (~ 7.7 wt. %), so, the cyclability of the double coated SnO_2 hollow spheres are well optimized in this coating conditions. This means the hydrothermally carbon coating and further graphene modification is successfully adopted in porous SnO_2 hollow morphology.

2.5. References

1. K. Amine, I. Belharouak, Z. Chen, T. Tran, H. Yumoto, N. Ota, S.-T. Myung, and Y.-K. Sun, "Nanostructured Anode Material for High-Power Battery System in Electric Vehicles," *Adv. Mater.* **22**, 3052 (2010).
2. R. Wang, C. Xu, J. Sun, L. Gao, and H. Yao, "Solvothermal-Induced 3D Macroscopic SnO_2/Nitrogen-Doped Graphene Aerogels for High Capacity and Long-Life Lithium Storage," *ACS Appl. Mater. Interfaces* **6**, 3427 (2014).
3. S. Yang, W. Yue, J. Zhu, Y. Ren, and X. Yang, "Graphene-Based Mesoporous SnO_2 with Enhanced Electrochemical Performance for Lithium-Ion Batteries," *Adv. Funct. Mater.* **23**, 3570 (2013).
4. C. Xu, J. Sun, and L. Gao, "Direct Growth of Monodisperse SnO_2 Nanorods on Graphene as High Capacity Anode Materials for Lithium Ion Batteries," *J. Mater. Chem*. **22**, 975 (2012).
5. S.-K. Park, S.-H. Yu, N. Pinna, S. Woo, B. Jang, Y.-H. Chung, Y.-H. Cho, Y.-E. Sung, and Y. Piao, "Facile Hydrazine-Assisted Hydrothermal Method for the Deposition of Monodisperse SnO_2 Nanoparticles onto Graphene for Lithium Ion Batteries," *J. Mater. Chem*. **22**, 2520 (2012).
6. K. T. Lee, Y. S. Jung, and S. M. Oh, "Synthesis of Tin-Encapsulated Spherical Hollow Carbon for Anode Material in Lithium Secondary Batteries," *J. Am. Chem. Soc*. **125**, 5652 (2003).
7. C. Kim, M. Noh, M. Choi, J. Cho, and B. Park, "Critical Size of a Nano SnO_2 Electrode for Li-Secondary Battery," *Chem. Mater*. **17**, 3297 (2005).
8. Z. Wen, X. Wang, S. Mao, Z. Bo, H. Kim, S. Cui, G. Lu, X. Feng, and J. Chen, "Crumpled Nitrogen-Doped Graphene Nanosheets with Ultrahigh Pore Volume for High-Performance Supercapacitor," *Adv. Mater*. **24**, 5610 (2012).

9. X. W Lou, Y. Wang, C. Yuan, J. Y. Lee, and L. A. Archer, "Template-Free Synthesis of SnO_2 Hollow Nanostructures with High Lithium Storage Capacity," *Adv. Mater*. **18**, 2325 (2006).
10. M. Noh, Y. Hwon, H. Lee, J. Cho, Y. Kim, and M. G. Kim, "Amorphous Carbon-Coated Tin Anode Material for Lithium Secondary Battery," *Chem. Mater.* **17**, 1926 (2005).
11. W. S. Hummers and R. E. Offeman, "Processable Aqueous Dispersions of Graphene Nanosheets," *J. Am. Chem. Soc.* **80**, 1339 (1958)
12. S. Yang, X. Feng, S. Ivanovici, and K. Mullen "Fabrication of Graphene-Encapsulated Oxide Nanoparticles: Towards High-Performance Anode Materials for Lithium Storage," *Angew. Chem. Int. Ed.* **49**, 8408 (2010).
13. T. Moon, C. Kim, S.-T. Hwang, and B. Park, "Electrochemical Properties of Disordered-Carbon-Coated SnO_2 Nanoparticles for Li Rechargeable Batteries," *Electrochem. Solid-State Lett.* **9**, A408 (2006).
14. T. Kim, J. Oh, B. Park, and K. S. Hong, "Correlation between Strain and Dielectric Properties in $ZrTiO_4$ Thin Films," *Appl. Phys. Lett*. **76**, 3043 (2000).
15. D. Son, D.-R. Jung, J. Kim, T. Moon, C. Kim, and B. Park, "Synthesis and Photoluminescence of Mn-Doped Zinc Sulfide Nanoparticles," *Appl. Phys. Lett*. **90**, 101910 (2007).
16. D.-R. Jung, D. Son, J. Kim, C. Kim, and B. Park, "Highly-Luminescent Surface-Passivated ZnS:Mn Nanoparticles by a Simple One-Step Synthesis," *Appl. Phys. Lett*. **93**, 163188 (2008).
17. X. Zhou, Y.-X. Yin, L.-J. Wan, and Y.-G. Guo, "A robust composite of SnO_2 hollow nanopsheres enwrapped by graphene as a high-capacity anode material for lithium-ion batteries," *J. Mater. Chem.* **22**, 17456 (2012).
18. Y. Su, S. Li, D. Wu, F. Zhang, H. Liang, P. Gao, C. Cheng, and X. Feng, "Two-Dimensional Carbon-Coated Graphene/Metal Oxide Hybrids for Enhanced Lithium Storage," *ACS Nano* **6**, 8349 (2012)

19. G. Zhou, D.-W. Wang, L. Li, N. Li, F. Li, and H.-M. Cheng, "Nanosize SnO_2 Confined in the Porous Shells of Carbon Cages for Kinetically Efficient and Long-Term Lithium Storage," *Nanoscale* **5**, 1576 (2013).
20. B. Zhang, Q. B. Zheng, Z. D. Huang, S. W. Oh, and J. K. Kim, "SnO_2-Graphene-Carbon Nanotube Mixture for Anode Material with Improved Rate Capacities," *Carbon* **49**, 4524 (2011).
21. X. W. Lou, C. M. Li, and L. A. Archer, "Designed Synthesis of Coaxial SnO_2@carbon Hollow Nanospheres for Highly Reversible Lithium Storage," *Adv. Mater.* **21**, 2536 (2009).
22. X. Zhou, L.-J. Wan, and Y.-G. Guo, "Binding SnO_2 Nanocrystals in Nitrogen-Doped Graphene Sheets as Anode Materials for Lithium-Ion Batteries," *Adv. Mater*. **25**, 2152 (2013).
23. Y. Wang, H. C. Zeng, and J. Y. Lee, "Highly Reversible Lithium Storage in Porous SnO_2 Nanotubes with Coaxially Grown Carbon Nanotube Overlayers," *Adv. Mater*. **18**, 645 (2006).
24. X. Sun, J. Liu, and Y. Li, "Oxides@C Core-Shell Nanostructures: One-Pot Synthesis, Rational Conversion, and Li Storage Property," *Chem. Mater*. **18**, 3486 (2006).
25. D. Wang, R. Kou, D. Choi, Z. Yang, Z. Nie, J. Li, L. V. Saraf, D. Hu, J. Zhang, G. L. Graff, J. Liu, M .A. Pope, and I. A. Aksay, "Ternary Self-Assembly of Ordered Metal Oxide-Graphene Nanocomposites for Electrochemical Energy Storage," *ACS Nano* **4**, 1587 (2010).
26. X. Yu, S. Yang, B. Zhang, D. Shao, X. Dong, Y. Fang, J. Li, and H. Wang, "Controlled Synthesis of SnO_2@Carbon Core-Shell Nanochains as High-Performance Anodes for Lithium-Ion Batteries," *J. Mater. Chem.* **21**, 12295 (2011).
27. L. Wang, D. Wang, F.-X. Zhang, and J. Jin, "Protein-Inspired Synthesis of SnO_2 Nanocrystals with Controlled Carbon Nanocoating as Anode Materials for

Lithium-Ion Battery," *RSC Adv.* **3**, 1307 (2013).

28. S. Jing, F. Gu, J. Kong, C. Ma, P. S. Lee and C. Li, "Lithium storage improvement from hierarchical double-shelled SnO_2 hollow spheres," *RSC Adv.* **4**, 10450 (2014).
29. L. Zhan, H. B. Wu, B. Liu and X. W. (David) Lou, "Formation of porous SnO_2 microboxes via selective leaching for highly reversible lithium storage," *Energy Environ. Sci.* **7**, 1013 (2014).
30. H. Kim, S.-W. Kim, Y.-U. Park, H. J. Gwon, D.-H. Seo, Y. Kim, and K. Kang, "SnO_2/Graphene Composite with High Lithium Storage Capability for Lithium Rechargeable Batteries" *Nano Res*. **3**, 813 (2010).
31. A. Sivashanmugam, T. P. Kumar, N.G. Renganathan, S. Gopukumar, M. Wohlfahrt-Mehrens, and J. Garche, "Electrochemical Behavior of Sn/SnO_2 Mixtures for Use as Anode in Lithium Rechargeable Batteries," *J. Power Sources* **144**, 197 (2005).
32. X. W. Lou, J. S. Chen, P. Chen, and L. A. Archer, "One-Pot Synthesis of Carbon-Coated SnO_2 Nanocolloids with Improved Reversible Lithium Storage Properties," *Chem. Mater*. **21**, 2868 (2009).
33. S. Stankovich, D. A. Dikin, R. D. Piner, K. A. Kohlhaas, A. Kleinhammes, Y. Jia, Y. Wu, S. T. Nguyen, and R. S. Ruoff, "Synthesis of Graphene-Based Nanosheets via Chemical Reduction of Exfoliated Graphite Oxide," *Carbon* **45**, 1558 (2007).
34. V. C. Tung, M. J. Allen, Y. Yang, and R. B. Kaner, "High-throughput solution processing of large-scale graphene," *Nat. Nanotech.* **4**, 25 (2009).
35. J. I. Paredes, S. V.-Rodil, P. S.-Fernadez, A. M.-Alonso, and J. M. D. Tascon, "Atomic Force and Scanning Tunneling Microscopy Imaging of Graphene Nanosheets Derived from Graphite Oxide," *Langmuir* **25**, 5957 (2009).
36. D. Yang, A. Velamakanni, G. Bozoklu, S. Park, M. Stoller, R. D. Piner, S. Stankovich, I. Jung, D. A. Field, C. A. Ventrice Jr., R. S. Ruoff, "Chemical analysis of graphene oxide films after heat and chemical treatment by X-ray photoelectron and Micro-Raman spectroscopy," *Carbon* **47**, 145 (2009).

37. N. Mohanty, A. Nagaraja, J. Armesto, and V. Berry, "High-Throughput, Ultrafast Synthesis of Solution-Dispersed Graphene via a Facile Hydride Chemistry," *Small* **6**, 226 (2010).
38. V. Lee, L. Whittaker, C. Jaye, K. M. Baroudi, D. A. Fischer, and S. Banerjee, "Large-Area Chemically Modified Graphene Films: Electrophoretic Deposition and Characterization by Soft X-ray Absorption Spectroscopy," *Chem. Mater.* **21**, 3905 (2009).
39. S. Wnag, P. K. Ang, Z. Wang, A. L. L. Tang, J. T. L. Thong, and K. P. Loh, "High Mobility, Printable, and Solution-Processed Graphene Electronics," *Nano Lett.* **10**, 92 (2010).
40. C. Mattevi, G. Eda, S. Agboli, S. Miller, K. A. Mkhoyan, O. Ceilk, D. Mastrogiovanni, G. Granozzi, E. Garfunkel, and M. Chhowalla, "Evolution of Electrical, Chemical, and Structural Properties of Transparent and Conducting Chemically Derived Graphene Thin Films," *Adv. Funct. Mater.* **19**, 2577 (2009).
41. C.-Y. Su, Y. Xu, W. Zhang, J. Zhao, X. Tang, C.-H. Tsai, and L.-J. Li, "Electrical and Spectroscopic Characterizations of Ultra-Large Reduced Graphene Oxide Monolayers," *Chem. Mater.* **21**, 5674 (2009).
42. C. G.-Navarro, R. T. Weitz, A. M. Bittner, M. Scolari, A. Mews, M. Burghard, and K. Kern, "Electronic Transport Properties of Individual Chemically Reduced Graphene Oxide Sheets," *Nano Lett.* **7**, 3499 (2007).
43. H. Wnag, J. T. Robinson, X. Li, and H. Dai, "Solvothermal Reduction of Chemically Exfoliated Graphene Sheets," *J. Am. Chem. Soc.* **131**, 9910 (2009).
44. W. Chen, and L. Yan, "Preparation of graphene by a low-temperature thermal reduction at atmosphere pressure," *Nanoscale* **2**, 559 (2010).
45. J.-Y. Hwang, C.-C. Kuo, L.-C. Chen, and K.-H. Chen, "Correlating Defect Density with Carrier Mobility in Large-Scaled Graphene Films: Raman Spectral Signatures for the Estimation of Defect Density," *Nanotechnology* **21**, 465705 (2010).

46. L. Wang, G. C. Liang, X. Q. Ou, X. K. Zhi, J. P. Zhang, and J. Y. Cui, "Effect of Synthesis Temperature on the Properties of $LiFePO_4$/C Composites Prepared by Carbothermal Reduction," *J. Power Sources* **189**, 423 (2009).
47. R. Chen, T. Zhao, J. Lu, F. Wu, L. Li, J. Chen, G. Tan, Y. Ye, and K. Amine, "Graphene-Based Three-Dimensional Hierarchical Sandwich-type Architecture for High-Performance Li/S Batteries," *Nano Lett.* **13**, 4642 (2013).
48. S. Ding and X. W. (David) Lou, "SnO_2 nanosheet hollow spheres with improved lithium storage capabilities," *Nanoscale* **3**, 3586 (2011).
49. A. M. Tripathi and S. Mitra, "Green template-free synthesis of SnO_2 nanospheres - a physical understanding and electrochemistry," *RSC Adv.* **3**, 19423 (2013).
50. Y.-S. Lin, J.-G. Duh, and M.-H. Huan, "Shell-by-Shell Synthesis and Applications of Carbon-Coated SnO_2 Hollow Nanospheres in Lithium-Ion Battery," *J. Phys. Chem. C* **144**, 13136 (2010).
51. X. Zhou, Y.-X. Yin, L.-J. Wan, and Y.-G. Guo, "A robust composite of SnO_2 hollow nanopsheres enwrapped by graphene as a high-capacity anode material for lithium-ion batteries," *J. Mater. Chem.* **22**, 17456 (2012).
52. Y. Su, S. Li, D. Wu, F. Zhang, H. Liang, P. Gao, C. Cheng, and X. Feng, "Two-Dimensional Carbon-Coated Graphene/Metal Oxide Hybrids for Enhanced Lithium Storage," *ACS Nano* **6**, 8349 (2012).
53. S. J. Prabakar, Y.-H. Hwang, E.-G. Bae, S. Shim, D. Kim, M. S. Lah, K.-S. Sohn, and M. Pyo, "SnO_2/Graphene Composites with Self-Assembled Alternating Oxide and Amine Layers for High Li-Storage and Excellent Stability," *Adv. Mater.* **25**, 3307 (2013).

국문 초록

미래의 필수적인 에너지원으로서의 리튬 이차전지는 물리, 화학, 그리고 재료 분야에서의 중요한 이슈가 되고 있다. 휴대용 전자기기부터 미래의 전기 자동차까지 리튬 이차 전지의 응용이 에너지 분야의 가장 중요한 연구 부분이다. 이번 논문 에서는 이러한 리튬 이차 전지의 성능을 결정하는데 가장 큰 영향을 미치는 전극 물질에 대한 연구를 하였다. 그 중 탄소를 대체할 차세대 음극 물질로서 주석 산화물에 대한 연구를 진행하였다.

1 장에서는 여태까지 진행되었던 음극물질로써 주석산화물에 대한 내용 정리하였다. 부피 팽창이 전극 특성에 문제가 되는 합금계열 물질들은 그 나노 구조를 바꾸거나 카본 물질과 복합재를 형성하여 큰 사이클 특성 향상을 보고 있다.

2 장에서는 기존에 보고된 나노 구조 중에서 주석 산화물 중공구에 비정질 카본과 그라핀을 이중 코팅해 음극 전극에 응용한 연구에 관한 내용이다. 빈 공간을 가지는 주석 산화물에 낮은 함량의 카본을 각각 다른 종류의 카본 물질을 코팅해 그 특성을

비교하였으며, 이를 높은 전류밀도와 낮은 전압 범위에서도 100 사이클 동안 이중 코팅한 물질이 적절한 용량이 나옴을 확인하였다.

주요어: 주석산화물, 중공구, 음극물질, 리튬 이차 전지 비정질 카본, 환원된 산화 그래핀.

학번: 2013-20610